Journal of
Composites Science

MDPI

Article

Analytical Modeling Approaches for the Cyclic Behavior of Concrete-Filled Circular Filament Wounded GFRP Tube Columns

Sajan Shakya * and Alexandra Hain *

Department of Civil and Environmental Engineering, University of Connecticut, 261 Glenbrook Rd., Storrs, CT 06269, USA
* Correspondence: sajan.shakya@uconn.edu (S.S.); alexandra.hain@uconn.edu (A.H.)

Abstract: Concrete-filled fiber-reinforced polymer (FRP) tubes (CFFTs) offer an alternative to traditional reinforced concrete columns for new construction applications due to their high strength, ductility, and corrosion resistance properties. Despite their popularity, there is a lack of accurate analytical models for the cyclic/seismic performance of CFFT columns. This is due to the absence of precise stress–strain models for FRP tubes and confined concrete under cyclic loading. Previous experiments on CFFT columns suggest that even minimal reinforcement ($\leq$1%) provides essential energy dissipation for extreme events. However, existing stress–strain models for FRP-confined concrete often neglect the contribution of longitudinal and transverse steel reinforcement. While some researchers have proposed material models to address this issue, the analytical modeling of confinement effects from both steel reinforcement and FRP tubes, especially under lateral cyclic loading, continues to pose a significant challenge. This study aims to use previously collected experimental data to evaluate current analytical modeling approaches in OpenSeesPy3.5.1.12 to simulate the lateral cyclic behavior of CFFT columns with $\pm$55° glass fiber-reinforced polymer (GFRP) fiber orientation. Both the lumped inelasticity and the distributed inelasticity modeling approaches are applied. The performance of various FRP confinement models is compared. The effect of plastic hinge length is also considered in the lumped plasticity approach. The findings suggest that integrating a fiber element section into the plastic hinge zone enhances the efficiency of the distributed inelasticity approach. This method accurately captures the non-linear behavior in the critical region and precisely predicts the shape of the hysteretic curve, all while reducing computational costs. Conversely, the lumped inelasticity modeling approach effectively forecasts energy dissipation and peak load values across the entire cyclic hysteresis curve, offering significant computational savings. Finally, a generalized modeling methodology for predicting the response of CFFTs under cyclic lateral load is proposed and subsequently validated using experimental results found in the existing literature.

Keywords: FRP confined concrete; OpenSeesPy modeling; distributed and lumped inelasticity modeling approaches; GFRP; 55° fiber orientation

Citation: Shakya, S.; Hain, A. Analytical Modeling Approaches for the Cyclic Behavior of Concrete-Filled Circular Filament Wounded GFRP Tube Columns. *J. Compos. Sci.* **2024**, *8*, 259. https://doi.org/10.3390/jcs8070259

Academic Editor: Francesco Tornabene

Received: 22 May 2024
Revised: 16 June 2024
Accepted: 2 July 2024
Published: 4 July 2024

1. Introduction

Fiber-reinforced composites have become popular in the field of civil engineering in recent decades due to their high specific strength, ductility, stiffness, and excellent resistance to corrosion [1]. Concrete-filled fiber-reinforced polymer (FRP) tubes (CFFTs) offer a practical substitute for traditional reinforced concrete columns in new construction projects, mainly in bridge substructures [2–7]. A CFFT comprises a prefabricated FRP tube and an encased concrete core. The FRP shell serves a dual function: it shields the internal concrete from environmental degradation and eliminates the requirement for traditional formwork and scaffolding, streamlining the construction process. Furthermore, FRP encasement contributes to the structural integrity of the column by offering both longitudinal and hoop reinforcement. Experimental studies have shown the promising

response of CFFT columns under reverse cyclic lateral loading and seismic loading. In particular, they have indicated that a minimal amount of internal steel reinforcement, even that below 1%, can impart the required energy dissipation characteristics to withstand extreme events [8].

Despite their potential as evidenced by decades of experimental and analytical work [9–14], there is a lack of accurate predictive models for the cyclic/seismic performance of CFFT columns. This is in part due to the lack of generalized models for the stress and strain response of FRP tubes and FRP-confined concrete, due to the wide variety of materials and fabrication procedures used to construct the FRP tube. The level of confinement and performance of an FRP composite heavily depends on the nature of the fiber, matrix, winding angle, and shell thickness. Additionally, the development of a reliable hysteretic damage model during cyclic loading poses a challenge in the current research landscape.

Several stress–strain models for FRP-confined concrete [15–22] have been developed and evaluated in the literature. The models proposed by Samman [15], Saiidi [16], Youseff [17], and Teng [20] are popular and have been validated against experimental data. Ozbakkaloglu [23] completed a comprehensive review of 88 such models and concluded that the accuracy of the models that make use of the hoop rupture strains ($\varepsilon_{h,rup}$) are, in general, significantly higher than the models that directly use the ultimate tensile strain of fibers (ε_f). Furthermore, the ultimate strain measured on the FRP shell at the time of FRP hoop rupture ($\varepsilon_{h,rup}$) is lower than the ultimate tensile strain of the fibers (ε_f) or FRP material (ε_{frp}) [20]. Pessiki [24] concluded that most of the better-performing models employ rupture strain efficiency factors (k_e) in their expression. Jiang [21,22] discovered that the stress–strain behavior of concrete confined by an FRP composite is affected by the type and size of the aggregates used in the concrete and proposed an innovative method to model the stress–strain relationship of FRP-confined concrete, considering the effect of aggregate size. The impressive impact resistance of polymer-based systems was highlighted in a broad review of the experimental, analytical, and numerical investigations conducted on the dynamic behavior of sandwich structures by Guo et al. [25]. Fahmy [26] examined the accuracy of 14 design-oriented stress–strain models of FRP-confined concrete from the available literature to predict the cyclic responses of columns subjected to both constant axial loading and cyclic lateral loading and concluded that the general response of an FRP-confined RC column to cyclic loading could be predicted using design-oriented stress–strain models.

A current gap in the literature is that most existing models for the compressive strength of confined concrete primarily focus on the increased strength and ductility offered by FRPs and overlook the contribution of longitudinal and transverse steel reinforcement within the column's cross-section. Megalooikonomou [27] attempted to address the combined contribution of the FRP shell and steel stirrups to predict the behavior of RC columns retrofitted with FRP jacketing. This model was later added to the source code of OpenSeesPy. However, this model has limitations for use in the CFFT columns that will be discussed in this study. Thus, the analytical modeling of the CFFT columns considering confinement effects from both steel reinforcement and FRP tubes under lateral cyclic loading remains a complex task.

This study evaluates the applicability of different analytical modeling approaches using the FEA software OpenSeesPy3.5.1.12 to simulate the cyclic lateral behavior of CFFT columns. The study focuses on CFFTs with $\pm 55^{\circ}$ glass fiber-reinforced polymer (GFRP) tubes constructed with filament winding. The first step was to use previously collected experimental data to evaluate the current analytical modeling approaches in OpenSeesPy3.5.1.12. Both the lumped inelasticity and distributed inelasticity modeling approaches were applied to compare the performance of various FRP confinement models. The distributed inelasticity modeling approach allows for nonlinearity at any section of the element. In contrast, the lumped plasticity modeling method assumes nonlinear behaviors at the ends of the structural element, with the body treated as elastic [28–32]. While applying the lumped plasticity modeling approach, different models and mathematical equations

available in the literature were employed to determine the length of the plastic hinge [33–37]. The influence of internal steel reinforcements was addressed in the modeling using the FRP confined concrete material model in OpenSeesPy developed by Megalooikonomou [27] and the results were compared with those from other confinement models. Finally, a generalized modeling approach is suggested and subsequently validated using experimental results found in the literature.

2. Stress–Strain Models for FRP Confined Concrete

When concrete is confined by an FRP tube, several mechanical properties (strength, ductility, and stiffness) are enhanced, making the material more promising for resisting applied loads. Along with increased compressive strength, confinement also positively impacts tensile strength. In this study, different confinement models from the literature are explored. The Samaan [15], Saiidi [16], and Teng [20] models focus solely on FRP confinement effects, while Megalooikonomou's model [27], which was originally developed for FRP retrofitting, considers both FRP confinement and internal reinforcement effects. For the tensile behavior of FRP-confined concrete, a model proposed by Yassin [38] and modified by Teng [39] for unconfined concrete is implemented. The following sections will review each of the FRP confinement models evaluated in this work.

2.1. Samaan Confinement Model

Samaan [15] introduced a straightforward framework for predicting the comprehensive bilinear stress–strain behavior of FRP-confined concrete, which is based on a connection between the dilation rate of concrete and the hoop stiffness of the restraining element. The model's parameters are linked to the material characteristics of the FRP shell and the concrete core. To depict the bilinear response of FRP-confined concrete, the four-parameter relationship formulated by Richard and Abbott in 1975 [40] was employed and adjusted as follows:

$$f_c = \frac{(E_1 - E_2)\varepsilon_c}{\left[1+\left(\frac{(E_1-E_2)\varepsilon_c}{f_0}\right)^n\right]^{\frac{1}{n}}} + E_2\varepsilon_c \quad (1)$$

where ε_c and f_c are the axial strain and stress of concrete, respectively, E_1 and E_2 are the first and second slopes, respectively, f_0 is the reference plastic stress at the intercept of the second slope with the stress axis, and n is a curve-shaped parameter that mainly controls the curvature in the transition zone whose value was taken as 1.5. These basic parameters are shown in Figure 1.

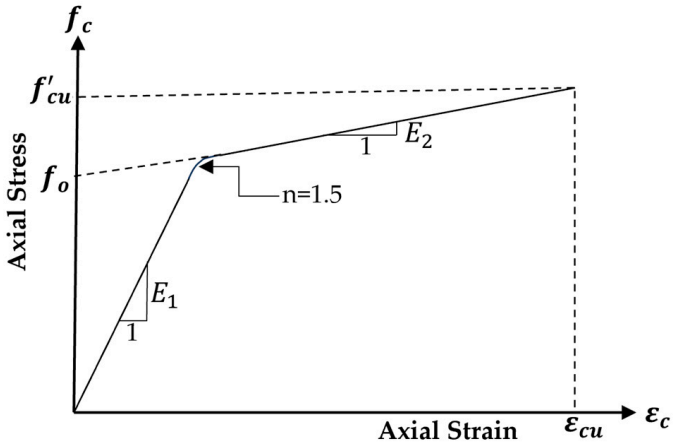

Figure 1. The bilinear confinement model proposed by Samaan [15].

The first slope of the confined concrete was calculated using Equation (2) as proposed by Ahmad and Shah [41,42]:

$$E_1 = 3950\sqrt{f'_{co}} \quad (2)$$

where f'_{co} is the unconfined compressive strength of concrete. Similarly, the second slope was defined as a function of the stiffness of the confining tube E_{frp} and, to a lesser extent, the unconfined strength of the concrete core as:

$$E_2 = 245.61 {f'_{co}}^{0.2} + 1.3456 \left(\frac{E_{frp} t_{frp}}{D} \right) \quad (3)$$

where t_{frp} is the thickness of the FRP tube and D is the core diameter. The intercept stress is a function of the strength of unconfined concrete and the confining pressure provided by the tube and was estimated as:

$$f_o = 0.872 f'_{co} + 0.371 f_r + 6.258 \quad (4)$$

where $f_r = \frac{2 f_{frp} t_{frp}}{D}$ is the confinement pressure with f_{frp} being the hoop strength of the tube. Furthermore, the ultimate strength of confined concrete can be related to the confining pressure by the relation:

$$f'_{cu} = f'_{co} + 6.0 f_r^{0.7} \quad (5)$$

and the ultimate strength, i.e., the point at which the response is terminated, was determined from the geometry of the bilinear curve as:

$$\varepsilon_{cu} = \frac{f'_{cc} - f_o}{E_2} \quad (6)$$

2.2. Saiidi Confinement Model

Saiidi [16] proposed a simple bilinear confinement model for computing concrete characteristics in reinforced concrete elements confined by carbon-fiber-reinforced plastic sheets. This model has since been applied to GFRP-confined concrete [4]. In a bi-linear curve, the first line terminates at the first peak stress defined by:

$$f'_{c1} = f'_{co} + 0.003 \frac{2 E_f t_f}{D} \quad (7)$$

and the strain by $\varepsilon_{c1} = 0.002$, where f'_{co} is the unconfined compressive strength of concrete, E_f is the effective modulus of elasticity of the tube in the hoop direction, t_f is the thickness of the FRP tube, and D is the core diameter. This line was followed by the second straight line that extends until the ultimate condition:

$$f'_{cc} = f'_{co} + 6.2 f_r^{0.7} \quad (8)$$

$$\varepsilon_{cu} = \frac{\varepsilon_{h,rup}}{0.1 - 0.25 \ln\left(\frac{f_r}{f'_{co}}\right)} \quad (9)$$

where $\varepsilon_{h,rup}$ is the rupture hoop strain of the FRP tube, $f_r = \frac{2 E_f \varepsilon_f t_f}{D}$ is the confinement pressure, f'_{cc} is the ultimate stress, and ε_{cu} is the ultimate strain. The confinement pressure f_r for circular and rectangular sections is found using ε_f = 50% of the failure strain of CFRP in the fiber direction.

2.3. Teng Confinement Model

The design-oriented stress–strain model was proposed by Lam and Teng [19] for FRP-confined concrete under axial compression. Teng [20] refined the model by updating the expressions for finding the ultimate axial strain and the compressive strength. The effects of confinement stiffness (E) and the jacket strain capacity (ε) were separately reflected and accounted for explicitly instead of having it reflected only through the confinement ratio.

The modified second version of Lam and Teng's model captures the stress–strain curves with both ascending and descending post-peak branches as shown in Figure 2. Teng [20] defined the basic ratios, namely confinement ratio $\frac{f_l}{f'_{co}}$, confinement stiffness ratio ρ_k, and strain ratio ρ_ε as given by the Equations (10)–(12):

$$\frac{f_l}{f'_{co}} = \frac{2E_f t_f \varepsilon_{h,rup}}{f'_{co} D} = \rho_k \rho_\varepsilon \tag{10}$$

$$\rho_k = \frac{2E_f t_f}{(f'_{co}/\varepsilon_{co})D} \tag{11}$$

$$\rho_\varepsilon = \frac{\varepsilon_{h,rup}}{\varepsilon_{co}} \tag{12}$$

where f_l is the confining pressure provided by the FRP jacket when it fails by rupture due to hoop tensile stresses, i.e., the maximum confining pressure possible with the jacket, f'_{co} is the unconfined compressive strength of concrete, and E_f, t_f, and $\varepsilon_{h,rup}$ are the effective modulus of elasticity in the hoop direction, thickness, and the rupture hoop strain of the FRP tube, respectively.

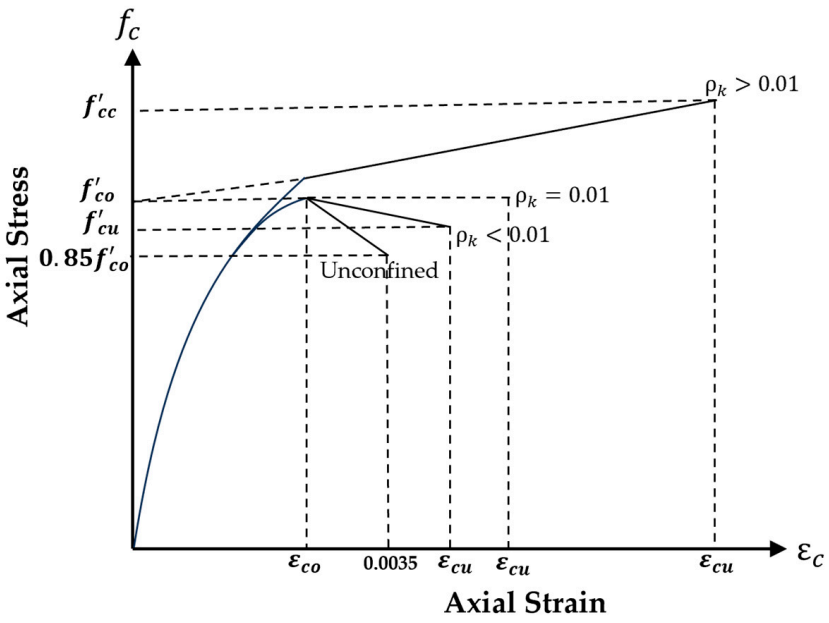

Figure 2. Schematic of a refined version of the modified Lam and Teng model [20]. The behavior following the yield point varies based on the confinement stiffness ratio ρ_k. Concrete that is adequately confined, with $\rho_k \geq 0.01$, exhibits a hardening behavior. On the other hand, for concrete that is not sufficiently confined, $\rho_k < 0.01$ shows a softening behavior.

In this refined version, the parabolic first portion of Lam and Teng's model remained unchanged and was governed by Equation (13):

$$f_c = E_c \varepsilon_c - \frac{(E_c - E_2)^2}{4f'_{co}} \varepsilon_c^2 \quad \text{for } 0 \leq \varepsilon_c \leq \varepsilon_{c1} \tag{13}$$

whereas the linear second portion was modified and was defined as:

$$f_c = f'_{co} + E_2 \varepsilon_c \text{ if } \rho_k \geq 0.01 \text{ with } \varepsilon_{c1} < \varepsilon_c \leq \varepsilon_{cu} \tag{14}$$

$$f_c = f'_{co} - \frac{f'_{co} - f'_{cu}}{\varepsilon_{cu} - \varepsilon_{co}}(\varepsilon_c - \varepsilon_{co}) \text{ if } \rho_k < 0.01 \text{ with } \varepsilon_{c1} < \varepsilon_c \leq \varepsilon_{cu} \quad (15)$$

Similarly, the improved equation for the ultimate axial strain of FRP-confined concrete was proposed as:

$$\frac{\varepsilon_{cu}}{\varepsilon_{co}} = 1.75 + 6.5\rho_k^{0.8}\rho_\varepsilon^{1.45} \quad (16)$$

where E_c is the elastic modulus of unconfined concrete; f_c and ε_c are the axial stress and the axial strain, respectively; E_2 = the slope of the linear second portion; $\varepsilon_{c1} = \frac{2f'_{co}}{E_c - E_2}$ is the smooth transition point where the parabolic first portion meets the linear second portion; ε_{cu} is the ultimate axial strain; f'_{cu} is the ultimate axial strain; and ε_{co} is the strain of concrete at the transition point.

2.4. Megalooikonomou's Confinement Model

Megalooikonomou [27] proposed a new material model for FRP-confined concrete considering the confining effect of the existing steel reinforcement for the retrofit of RC columns with FRP jacketing. This model was added to the source code of OpenSeesPy as a uniaxial material, i.e., the 'FRPConfinedConcrete' material. To date, the model has no tensile strength and uses the degraded linear unloading/reloading stiffness in the case of cyclic loadings based on the work of Karsan and Jirsa [43]. The FRP-confined concrete model proposal by 'Federation Internationale du Beton' (fib) [44] was enhanced to consider the confining effect of the existing steel reinforcement to develop the material model based on an iterative procedure in which pressure coming from the FRP jacket was initially assumed. The Poisson's coefficient up to the yielding of steel stirrups and the pressure coming from the steel ties were calculated based on the Braga–Gigliotti–Laterza (BGL) model [45]. The confining pressure in the concrete core results from the combined lateral pressures exerted by both the FRP and steel confining systems. The critical step occurs during the final stage, where the jacket's confining pressure is determined based on the circumferential strain obtained from the following Equation (17):

$$\varepsilon_c = \frac{\Delta C}{C} = \frac{R_{core}(1 + \varepsilon_{r,core}) + c(1 + \varepsilon_{r,cover})}{R_{core} + C} - 1 \quad (17)$$

The model considers the dilation of concrete under compression and the buckling of longitudinal bars as two conditions of failure. Failure is predicted by comparing the circumferential strain due to these conditions with the deformation capacity of FRP tensile coupons. Ensuring compatibility of strain in the lateral direction between the jacketing system and the encased concrete is crucial. Ultimately, the bilinear stress–strain response of FRP-confined concrete culminates in jacket rupture either due to hoop strains surpassing the material's strain capacity or interaction with buckled longitudinal bars. This model can be applied to FRP-confined concrete columns without lateral ties, like how other confinement models disregard lateral tie confinement.

Based on the observed confinement models, it can be inferred that the longitudinal tensile elastic modulus, ultimate tensile strength, and rupture hoop strain of the FRP tube play crucial roles in accurately defining FRP confined concrete. These parameters highly depend on the fiber angle.

3. Baseline Experimental Study

The baseline experiment used to evaluate the modeling approaches of this study is the work by Zhu [10] in which both monotonic and lateral cyclic loading were applied on the CFFT column (GFRP tube with ±55° orientation and filament winding). Zhu [10] conducted tests on a control RC column and three different types of CFFT columns including a cast-in-place CFFT, a precast CFFT with grouted starter bars from the footing, and a precast CFFT

post-tensioned to the footing with internal threaded rods. In this study, the cast-in-place CFFT was used as a baseline. The specimen was subjected to testing with a constant axial load of 445 kN, representing the dead load from a bridge superstructure. Additionally, a cyclic lateral load was imposed to simulate seismic loading. The lateral load was applied using a displacement control, corresponding to a multiple of the first yield displacement of the internal steel in the control RC column, which occurred at 30 mm. Subsequently, the specimens were monotonically pushed to a displacement of 300 mm, equivalent to a 13.3% drift ratio.

The tubes, with an inside diameter of 312 mm and a wall thickness of 5.1 mm, were fabricated using filament winding with $\pm 55^{\circ}$ E-glass fibers and epoxy resin. All columns were 2.3 m tall and constructed using Y-series tubes. The unconfined compressive strength of the concrete in all columns was 55 MPa. Each column included four 16 mm (No. 5) and four 19 mm (No. 6) diameter Grade 414 MPa mild steel bars, except for the post-tensioned CFFT column. Figure 3 illustrates the section of the CFFT column and the loading protocol.

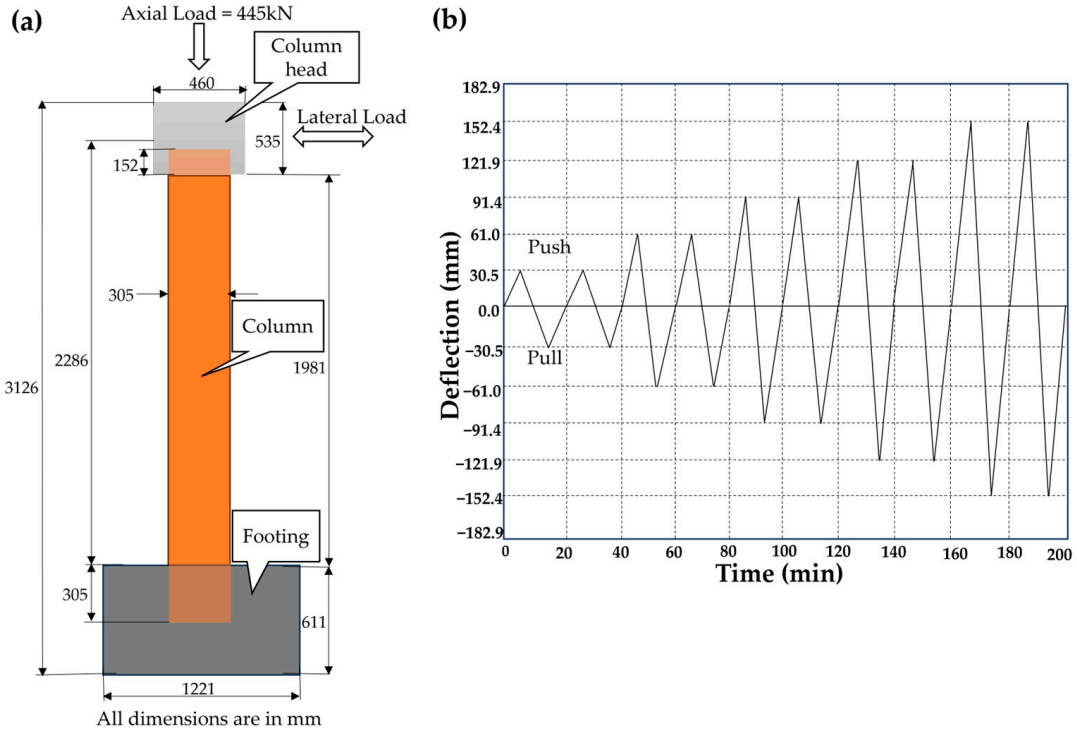

Figure 3. Experimental setup of the CFFT column by Zhu [10]. (**a**) CFFT column with dimensions and applied loading conditions and (**b**) reverse cyclic lateral loading protocol.

4. Analytical Modeling Approaches

The pseudo-static analysis of a CFFT column with a constant axial compression force and a reverse cyclic lateral load was carried out using the two most common nonlinear modeling approaches, namely distributed inelasticity, and lumped inelasticity/concentrated plasticity methods. The distributed inelasticity modeling approach was adopted in two ways in this study. The first with a fiber section applied to the full element length and the second with the fiber section assigned to the plastic hinge length [35]. Therefore, there are three approaches utilized altogether: Approach I, Approach II, and Approach III, which are displayed in Figure 4.

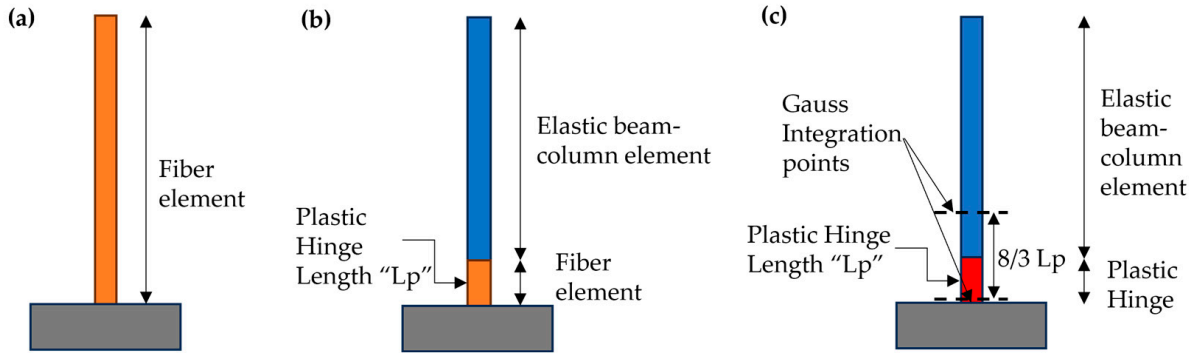

Figure 4. Inelasticity modeling approaches adopted in the study. (**a**) Approach I: Distributed Inelasticity Modeling Approach—Fiber section to the full length: Spread of plasticity/inelasticity behavior along the nonlinear beam–column element through full length, (**b**) Approach II: Distributed Inelasticity Modeling Approach—Fiber section to plastic hinge length: Spread of plasticity/inelasticity behavior along the nonlinear beam–column element at plastic hinge length, and (**c**) Approach III: Lumped Inelasticity Modeling Approach—HingeRadau beam integration: Concentrated plasticity at plastic hinge zone and elastic element for the remaining part.

Open-source software, OpenSeesPy3.5.1.12, was used for the nonlinear analysis of the CFFT columns. Concrete 02 and FRP-confined concrete were used as material models. As previously described, the confinement models compared were those of Samaan [15], Saiidi [16], Teng [20], and Megalooikonomou [27]. The unconfined concrete strength and Young's modulus of concrete were taken from the baseline experiment. Steel 02 was utilized to model the rebar reinforcement with yield stress, Young's modulus, and strain hardening reported in the baseline experiment. The longitudinal behavior of the GFRP tube was defined with the following stress–strain relationship, based on the manufacturer's data and coupon tests of Shao [46]:

$$\sigma_l = \frac{\varepsilon_l}{|\varepsilon_l|}\left(-21.24 + \sqrt{451.2 + 638,143\varepsilon_l}\right) \text{ for } |\varepsilon_l| \leq 0.05 \text{ (MPa)} \tag{18}$$

$$\sigma_l = \frac{\varepsilon_l}{|\varepsilon_l|}\left(-3.08 + \sqrt{9.49 + 13,423\varepsilon_l}\right) \text{ for } |\varepsilon_l| \leq 0.05 \text{ (ksi)} \tag{19}$$

where σ_l and ε_l are the longitudinal stress and strain of the FRP tube, respectively. The above relation was modeled using a tri-linear curve with 'uniaxialMaterial Hysteretic' material [47] to define the longitudinal behavior of FRP tubes. The pinching factor for strain, pinching factor for stress, damage due to ductility, damage due to energy, and degrading factor of unloading stiffness were taken as 1, 1, 0, 0, and 0.3, respectively.

P-Delta effects were considered through the P-Delta Coordinate Transformation, a geometric transformation that performs a linear geometric transformation of beam stiffness and resisting force from the basic system to the global coordinate system.

4.1. Distributed Inelasticity Modeling Approach

Numerical models based on distributed inelasticity consider the spread of plasticity/inelasticity behavior along the element defined by the fiber response. This method is one of the more accurate methods in performing the nonlinear analysis of structures [31]. In a fiber element model, the section and all of its components are discretized into finite fibers/parts, and at each fiber, a generic uniaxial constitutive behavior is defined. There is automatic integration of the P-M response and one can introduce P-M-V interaction if desired. However, it can be computationally expensive, especially when the structure consists of many elements, complex loading conditions, and complex constitutive relationships for the materials involved.

In Approach I, inelastic behavior was distributed across the entire length of the element. This was achieved using a force-based "NonlinearBeamColumn" element with a fiber section assigned to the full length, as depicted in Figure 4a. In Approach II, the inelasticity was concentrated over the plastic hinge length through a fiber section, while the remaining portion of the element was considered elastic, as shown in Figure 4b. Approach II still falls under the distributed inelasticity fiber element modeling approach as it specifically utilizes fiber section modeling for the finite length at the support zone of the CFFT column.

Five Gauss–Lobatto integration points were defined for the fiber element. The section was built using fiber section command with a patch for the concrete and FRP tube and a layer for steel reinforcement. The considered discretization of the column section is illustrated in Figure 5. Twelve radial and sixteen tangential divisions were employed for the concrete section. The column base was modeled as a fixed support.

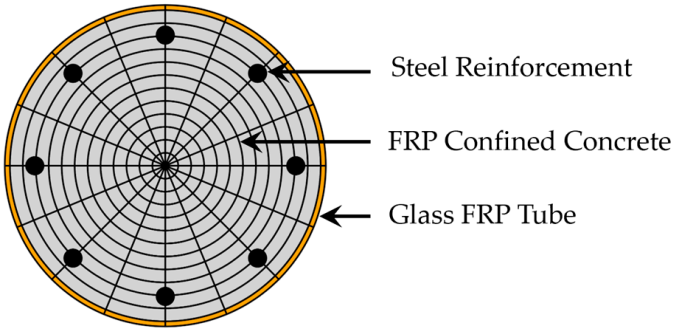

Figure 5. The fiber section considered in OpenSeesPy3.5.1.12 for analytical modeling.

4.2. Lumped Inelasticity/Concentrated Plasticity Modeling Approach

The plastic hinge modeling assumptions are computationally more efficient but require user knowledge on the calibration of the inelastic element parameters [31]. In Approach III, Hinge Radau beam integration, which is the modified two-point Gauss–Radau integration method developed by Michael H. Scott [28], was employed. Here, nonlinear behavior was lumped at the finite length toward the support end of the CFFT column while the body was modeled as elastic. Two integration points were placed over the hinge region, one at the element end and another at 8/3 of the hinge length inside the element as shown in Figure 4c.

This approach involved conducting moment curvature analysis on a fiber section created using the fiber section command with patches for concrete and FRP tubes and layers for steel reinforcement. The resulting moment–curvature curves were then linearized into three segments (Tri-linearization) to represent flexural behavior. A section aggregator was utilized to create a coupled section force-deformation model, incorporating axial deformation (addressed elastically), curvature from the tri-linearization, and shear deformation [48], all calculated based on constitutive material laws and section state determination.

FRP confinement impacts the plastic hinge length of CFFT columns, with tests indicating both increased and decreased plastic hinge lengths as compared to RC counterparts [33]. Researchers do not agree on how to measure the plastic hinge length (L_p) for FRP-confined columns. In this study, different plastic hinge length models available in the literature were employed and their effects on results were observed. The plastic hinge length in the literature includes equivalent plastic hinge length and physical plastic hinge length. All models and calculations in this study refer to equivalent plastic hinge lengths. Paulay and Priestley [35] proposed that, for traditional RC columns, the plastic hinge length (L_p) consists of two components:

$$L_p = \alpha L + \beta f_y d_b, \text{ but } L_p > 0.044 f_y d_b \quad (20)$$

where d_b is the diameter of the longitudinal tension reinforcement, α = 0.08, and β = 0.022. The first component of Equation (20) is the column bending component, and the second component accounts for the strain penetration component of the longitudinal reinforcement into the supporting base.

The general form of Equation (20) was adopted, and variation was made for CFFT columns to reflect the influence of FRP confinement by Gu [33] and proposed a discontinuous model for finding the plastic hinge length of the CFFT column based on analytical studies and regression of test results:

$$L_p = \left(0.59-2.3\lambda_f+2.28\lambda_f^2\right)L + 0.022 f_y d_b \text{ when } \lambda_f > 0.1 \quad (21)$$

where λ_f is the confinement ratio defined as the ratio of confinement pressure to unconfined concrete strength, L is the length of a cantilever column, and f_y and d_b are the yield strength and diameter of longitudinal steel bars, respectively.

Youssf [36] introduced an alternative model for the plastic hinge length (L_p) in CFFTs, where L_p is directly proportional to the confinement ratio:

$$L_p = 0.8\lambda_f L + 0.022 f_y d_b \quad (22)$$

This model utilizes the distribution of hoop strain along the column height to establish L_p. Specifically, L_p is determined as the height above the column footing where the measured FRP hoop strain values exceed one-third of the maximum strain recorded. This definition assumes a correlation between the hoop strain and the extent of the plastic hinge.

Another model of L_p allowing for FRP confinement was proposed by Yuan [37] using the FEM results and through regression analyses:

$$L_p = L_{p0}+L_{\text{pf}} = \left(0.08L + 0.022 f_y d_b\right) + 0.13\left(\frac{2r}{b}+0.2\right)^{0.1}\left(e^{-1.5\lambda_f}-e^{-40\lambda_f}\right)L \quad (23)$$

The first term $L_{p0} = 0.08L + 0.022 f_y d_b$ is the equivalent plastic hinge length for traditional unconfined RC columns, proposed by Paulay and Priestley [35]. The second term gives the effect of the confinement ratio on the equivalent plastic hinge length.

5. Comparison of Analysis Results with the Baseline Experimental Study

The first step in the investigation was to conduct monotonic pushover analyses for all modeling approaches and compare the results to the baseline experimental data. Full cyclic pushover analyses were then conducted and compared to the experimental data only for the modeling approaches that produced promising monotonic results in Step 1. Table 1 summarizes the approaches and models that were compared against the baseline experiment.

Table 1. Types of analysis performed on baseline experiment with different analytical and mathematical models adopted.

Analysis Type	Modeling Approach	Plastic Hinge Length Model	Concrete Confinement Model
Monotonic Pushover	(I) Distributed inelasticity modeling approach—Fiber section to full-length	-	Samaan [15] Saiidi [16] Teng [20] Megalooikonomou [27]
	(II) Distributed inelasticity modeling approach—Fiber section to plastic hinge length	Paulay and Priestley [35]	
	(III) Lumped inelasticity modeling approach using HingeRadau beam integration	Paulay and Priestley [35] Gu [33] Youssf [36] Yuan [37] Zaghi [4]	

Table 1. *Cont.*

Analysis Type	Modeling Approach	Plastic Hinge Length Model	Concrete Confinement Model
Full Cyclic Pushover	(I) Distributed inelasticity modeling approach—Fiber section to full-length	-	Saiidi [16] Teng [20]
	(II) Distributed inelasticity modeling approach—Fiber section to plastic hinge length	Paulay and Priestley [35]	
	(III) Lumped inelasticity modeling approach using HingeRadau beam integration	Paulay and Priestley [35] Youssf [36]	Saiidi [16] Teng [20] Megalooikonomou [27]

5.1. Monotonic Pushover Analysis

First, the monotonic pushover analyses were conducted under a displacement control mode using all three analytical modeling approaches. The performance of the modeling approaches, confinement models, and plastic hinge length was evaluated by comparing the load-displacement response from the models to the experimental data by Zhu [10].

Figure 6a shows that the predicted initial stiffness of the CFFT column in the elastic region is relatively higher compared to the experimental curve with the implementation of Approach I. Additionally, the analytical curves exhibit minimal hardening behavior in the plastic region with all the confinement models in Approach I. The elevated initial stiffness in the elastic zone and the minimal hardening behavior in the plastic hinge zone appear to be rectified through the implementation of Approach II, as seen in Figure 6b. Despite both Approach I and II employing the distributed inelasticity fiber element modeling method, the contrasting results observed in Figure 6a,b can be attributed to their different handling of non-linearity and stiffness distribution. The overestimated stiffness during the initial elastic phase by Approach I is due to its consideration of the entire cross-section, including the concrete core and the FRP jacket, in the fiber element section throughout the full length. But practically, the FRP provides passive confinement that is activated only when the Poisson's ratio of the concrete surpasses that of the FRP tube. In the plastic phase, this approach might underestimate stiffness because of overestimation of material damage and strain. Conversely, Approach II, which applies a fiber element section only to the plastic hinge zone and an elastic element to the remaining part, captures the non-linear behavior in the critical region more accurately while disregarding non-linearity in the rest of the structure. This results in a more precise representation of stiffness distribution, producing results that align more accurately with experimental data.

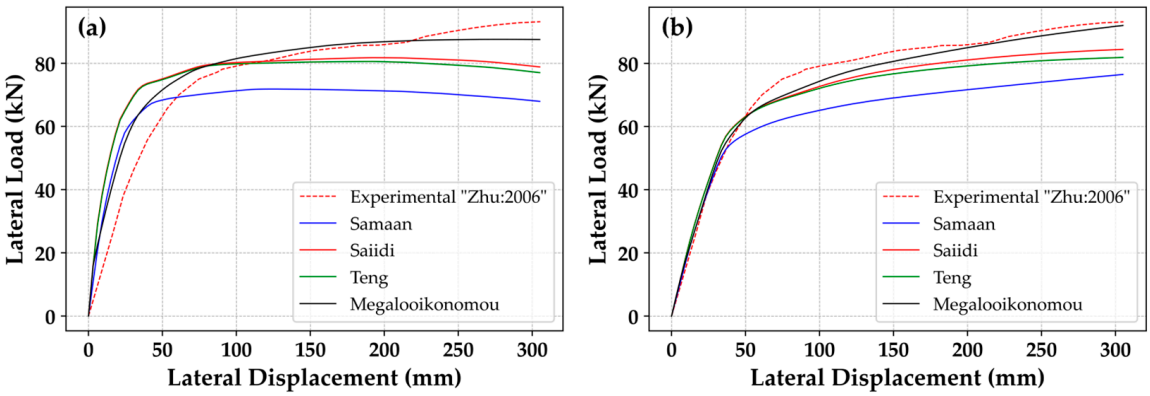

Figure 6. Comparison of the performance of different confinement models using the distributed inelasticity approach (fiber element modeling) with respect to the experimental monotonic curve by Zhu [10]. (**a**) Approach I and (**b**) Approach II.

With the application of the Megalooikonomou confinement model [27] and Approach II, the analytical monotonic curve matches the experimental curve perfectly as seen in

Figure 6b, but the model was found to be very sensitive and computationally expensive. This may be due to the consideration of internal steel reinforcement effects by Megalooikonomou [27] in the confinement. The predictions by Saiidi [16] and Teng [20] have good agreement but are slightly below the experimental curve which is likely caused by ignoring the confinement effects from the steel. The prediction by Samaan [15] is significantly below the experimental curve in both Approach I and II. As such, this confinement model was not considered for further analysis.

For Approach III, the moment–curvature analysis was performed in a fiber section using the Saiidi [16], Teng [20], and Megalooikonomou [27] confinement models. Figure 7 shows tri-linearization of the moment–curvature results representing flexural behavior that was coupled with axial and shear behavior using a section aggregator in OpenSeesPy3.5.1.12.

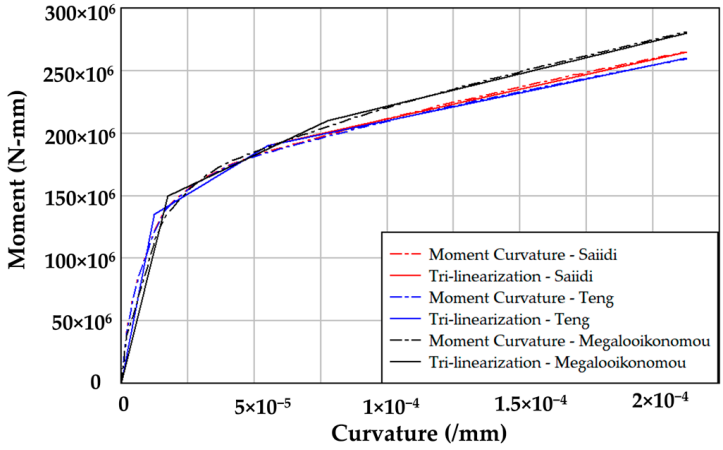

Figure 7. Tri-linearization of the moment curvatures of a fiber section using the Saiidi [16], Teng [20], and Megalooikonomou [27] confinement models.

Here, the length of the plastic hinge was calculated using four methods by Gu [33], Youssf [36], Yuan [37], and Paulay and Priestley [35] and one of the experimental shake table observations by Zaghi [4] and the results are displayed in Table 2.

Table 2. Plastic hinge lengths using various theories.

S.N.	Plastic Hinge Length Model	Plastic Hinge Length (L_p)—mm	L_p/D
1	Gu [33]	863	2.76
2	Youssf [36]	401	1.24
3	Yuan [37]	573	1.84
4	Paulay and Priestley [35]	329	1.05
5	Zaghi [4]	449	1.44

Approach III with plastic hinge length models by Gu [33], Yuan [37], and Zaghi [4] performed relatively poorly, as the predicted curves fall significantly below the experimental curve with the softening behavior as observed in Figure 8b,d,e. The plastic hinge lengths calculated using the Gu [33], Yuan [37], and Zaghi [4] models are 863 mm, 573 mm, and 449 mm, respectively, for the CFFT in the baseline experiment by Zhu [10]. However, when considering the 8/3Lp position for Gauss integration points as suggested by the Hinge Radau beam integration method as shown in Figure 4c, a value of 2300 mm is obtained from Gu [33], which exceeds the total element length of 2286 mm. Similarly, the Yuan model [37] yields a value of 1528 mm, covering more than 2/3 of the element length, and the Zaghi model [4] provides 1198 mm, surpassing half of the element length. These large plastic hinge zones generate the location of Gauss integration points to contradict the physical reality of plastic hinge behavior in the analytical model. Thus, the analytical results of the

lumped inelasticity approach with these plastic hinge lengths deviate from the experimental curves. Consequently, these plastic hinge length models were discarded for further cyclic loading analysis. The predictions with plastic hinge length models by Paulay and Priestley [35] with the Megalooikonomou confinement model [27] performed excellently with better computational efficiency as compared to the distributed inelasticity modeling approaches. However, this approach produces curves with only straight lines, which does not accurately capture the shape of the experimental response as seen in Figure 8.

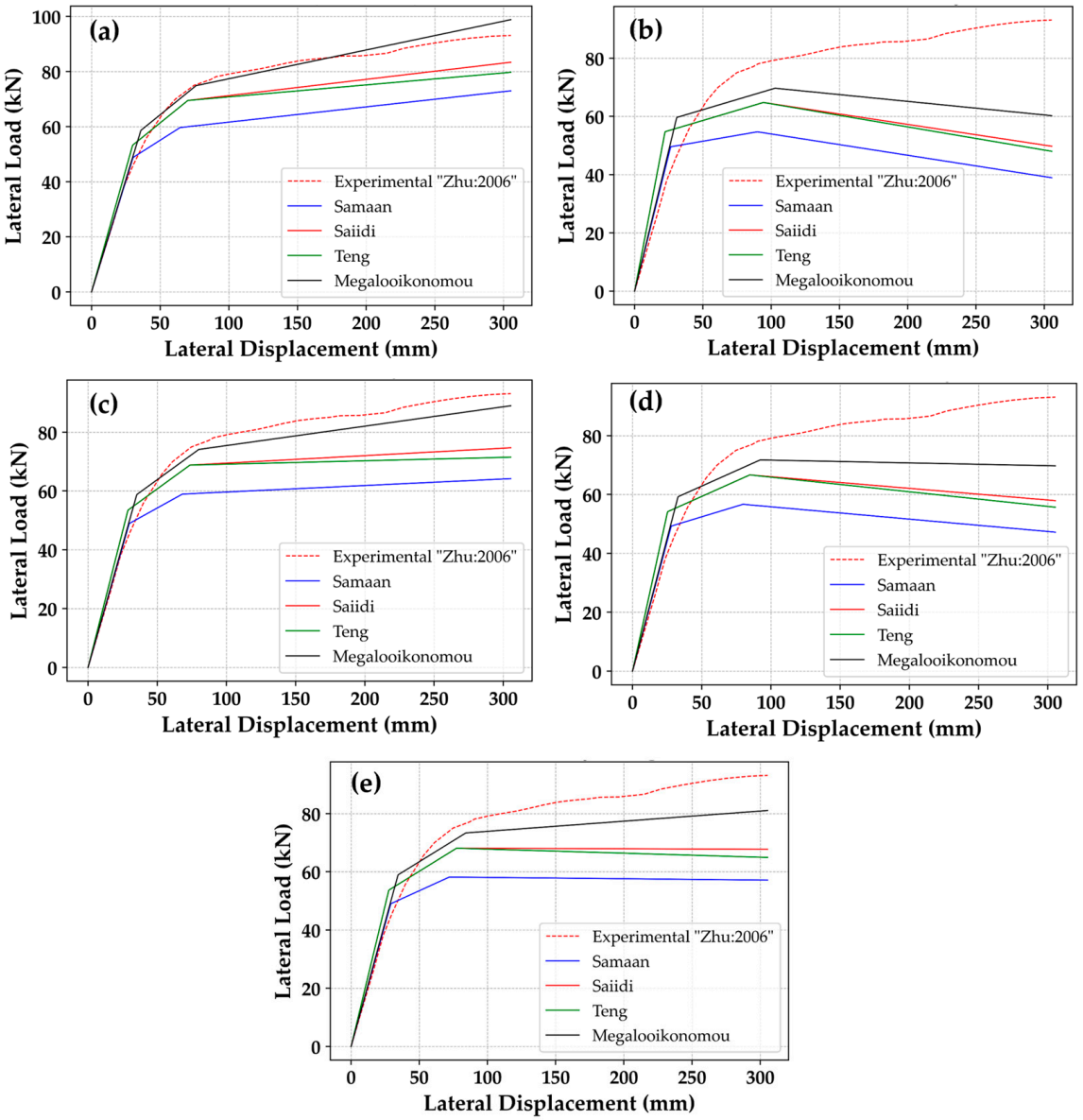

Figure 8. Comparison of performances of different confinement models using Approach III with respect to the experimental monotonic curve by Zhu [10]. Plastic hinge length models by (**a**) Paulay and Priestley [35], (**b**) Gu [33], (**c**) Youssf [36], and (**d**) Yuan [37] and (**e**) the Zaghi shake table test [4].

5.2. Full Cyclic Pushover Analysis

A full cyclic displacement-controlled pushover analysis was conducted to compare the analytical hysteretic curve with the experimental results using all three modeling approaches and promising confinement models and plastic hinge lengths presented in Table 1.

Figure 9 shows that the analytical hysteresis curves exhibit only a partial alignment with the experimental curve when using Approach I. This is due to the reasons mentioned in the explanations of monotonic curves in the previous section. Employing confinement models proposed by Saiidi [16] and Teng [20], the predicted peak load values were found to be 79.1 kN and 77.9 kN, respectively, both falling below the experimental value of 95 kN. However, the area enclosed by the analytical curve, i.e., energy dissipation, appears to be on the higher side. Specifically, the analytical enclosed areas for the Saiidi [16] and Teng [20] confinement models are 1.64 and 1.63 times greater than the experimental value of 86,052 kNmm. Interestingly, the model did not converge with the Megalooikonomou [27] confinement model during the full cyclic pushover analysis using Approach I.

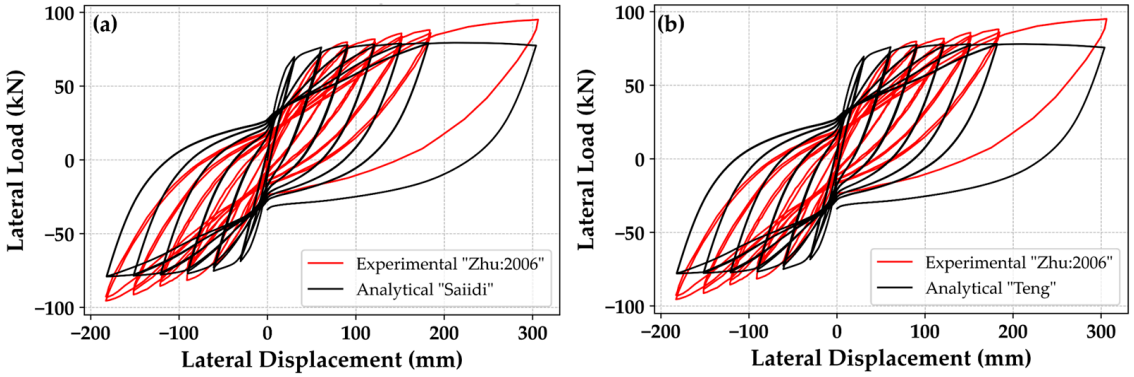

Figure 9. Comparison of the performance of the confinement models using Approach I with respect to the experimental full cyclic hysteretic curve by Zhu [10]. Performance of the (**a**) Saiidi [16] and (**b**) Teng [20] confinement models.

Figure 10 shows that the analytical hysteresis curves closely resemble the experimental curve when utilizing Approach II. By employing confinement models proposed by Saiidi [16] and Teng [20], the predicted peak load values increased to 91.0 kN and 89.3 kN, respectively. However, both values still fall slightly below the experimental value of 95 kN. In contrast, the energy dissipation from both confinement models is nearly the same, with it being 1.17 times greater than the experimental value of 86,052 kNmm. Thus, both peak loads and energy dissipation were more accurately predicted using Approach II as compared to Approach I. The model still did not converge with the Megalooikonomou [27] confinement model during the full cyclic pushover analysis using Approach II.

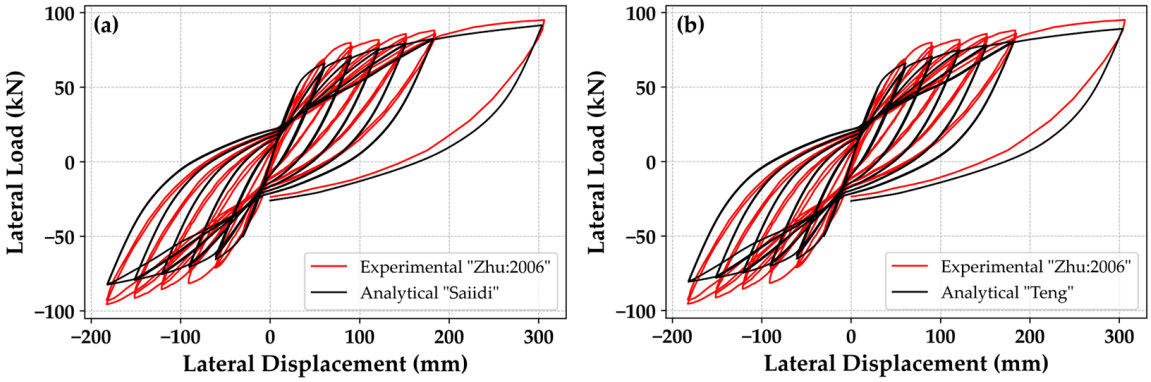

Figure 10. Comparison of the performance of the confinement models using Approach II with respect to the experimental full cyclic hysteretic curve by Zhu [10]. Performance of the (**a**) Saiidi [16] and (**b**) Teng [20] confinement models.

Approach III was implemented using the two plastic hinge length models, namely Paulay and Priestley [35] and Youssf [36], which showed good performance in the mono-

tonic pushover analysis. Figure 11c, which includes the analytical results of the Paulay and Priestley plastic hinge length model [35] and Megalooikonomou confinement model [27], shows the best agreement in matching the peak loads. The analytical result was 98 kN compared to the experimental peak lateral load value of 95 kN, a minor 3% error. The comparison of energy dissipation for this case is 77,716 kNmm for the analytical model compared to the experimental value of 86,052 kNmm, an 8.5% error. The optimal performance in terms of energy dissipation was achieved using the Teng confinement model [20], which reduces the error to 0.7%. However, this combination of Paulay and Priestley [35] hinge length and the Teng confinement model [20] underestimates the peak load by 9.5%, which can be attributed to the neglect of the impact of the transverse steel reinforcement.

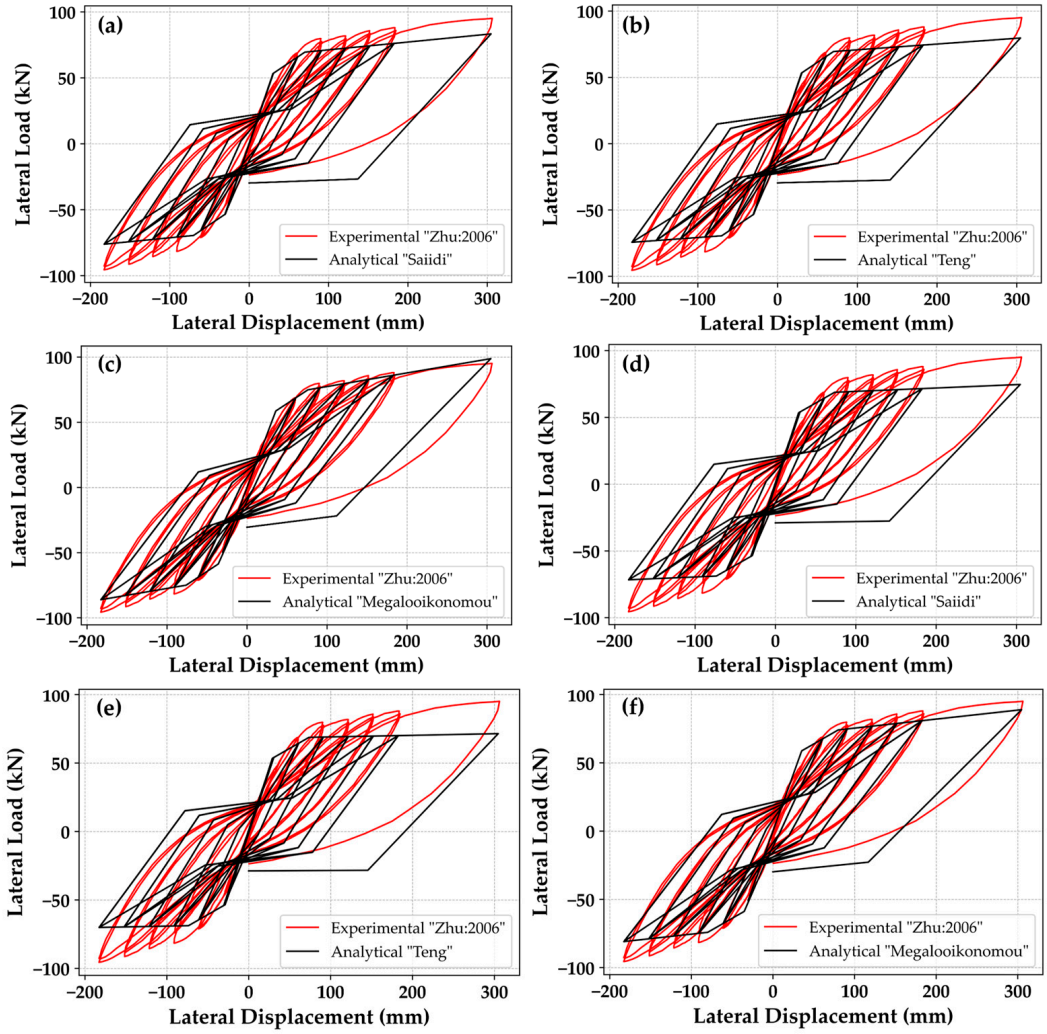

Figure 11. Comparison of the performance of promising confinement models using Approach III with respect to the experimental full cyclic hysteretic curve by Zhu [10]. Performance by the (**a**) Saiidi [16], (**b**) Teng [20], and (**c**) Megalooikonomou [27] confinement models with the Paulay and Priestley [35] plastic hinge length model. Performance by the (**d**) Saiidi [16], (**e**) Teng, and (**f**) Megalooikonomou [27] confinement models with the Youssf [36] plastic hinge length model.

Table 3 presents a detailed list of analytical values for the enclosed area within the full cyclic hysteretic loop that represents the dissipated energy. It was observed that when Approach III was utilized in conjunction with the Teng confinement model [20] and Paulay and Priestley plastic hinge length model [35], the enclosed area was predicted most accurately. In contrast, distributed inelasticity approaches tended to overpredict the energy dissipation.

Table 3. Analytical enclosed area within the hysteretic curves that represent the dissipated energy.

Modeling Approach	Concrete Confinement Model	Plastic Hinge Length Model	Cumulative Dissipated Energy (kNmm)
(I) Distributed inelasticity modeling approach—Fiber section to full-length	Saiidi [16]	-	141,096
	Teng [20]	-	140,403
(II) Distributed inelasticity modeling approach—Fiber section to plastic hinge length	Saiidi [16]	Paulay and Priestley [35]	100,523
	Teng [20]	Paulay and Priestley [35]	100,485
(III) Lumped inelasticity modeling approach using HingeRadau beam integration	Megalooikonomou [27]	Paulay and Priestley [35]	78,716
		Youssf [36]	79,097
	Saiidi [16]	Paulay and Priestley [35]	87,211
		Youssf [36]	87,414
	Teng [20]	Paulay and Priestley [35]	86,721
		Youssf [36]	87,020

6. Proposed Modeling Approach

Approach I and II, which involve distributed inelasticity modeling with the fiber section being assigned to the full element length and plastic hinge length, respectively, both capture the shape of the full cyclic hysteretic curve and monotonic behavior. Specifically, Approach II provides a precise representation of the stiffness distribution throughout the loading history, producing results that align more accurately with experimental data than those from Approach I. Approach III, which uses lumped inelasticity (concentrated plasticity modeling) with HingeRadau beam integration, is better suited for capturing peak loads, displacements, and dissipated energy when used with the Paulay and Priestly plastic hinge model [35]. However, Approach III does not fully represent the curve's shape due to the limitation of only using straight lines. The most promising model for predicting confined concrete strength, strain, and stiffness is the Teng confinement model [20]. In this study, it accurately predicted the hysteric shape and accumulated energy while maintaining computational efficiency.

Due to the limitations of the various approaches, a two-pronged modeling approach is suggested using Approach II and III to capture the shape of the cyclic response as well as the peak loads and energy dissipation, respectively. Both methods should employ the Paulay and Priestly plastic hinge model [35] and the Teng confinement model [20]. For more precise peak load prediction, the Megalooikonomou [27] confinement model can be employed in Approach III.

To negate the need for two separate modeling approaches, the stiffness and strength degradation rule in OpenSeesPy3.5.1.12 must be improved and a new concrete confinement model should be developed in OpenSeesPy3.5.1.12 for models like Megalooikonomou [27] that consider the contribution of steel reinforcement. In addition, the concentrated plasticity modeling approach is the best in terms of computational efficiency but hugely depends on the plastic hinge length. As researchers do not agree on generalized rules of plastic hinge lengths for CFFTs, a detailed investigation for CFFT columns is needed.

To further generalize the modeling approach, the authors suggest adopting the longitudinal backbone curve for the FRP tube adopted from Hain [49,50] which is shown in Figure 12. This curve was developed for $\pm 55^{\circ}$ GFRP fiber orientation constructed with filament winding. By suggesting general behavior for FRP material, the proposed modeling approaches can be used to inform experimental design when specific material properties may be missing.

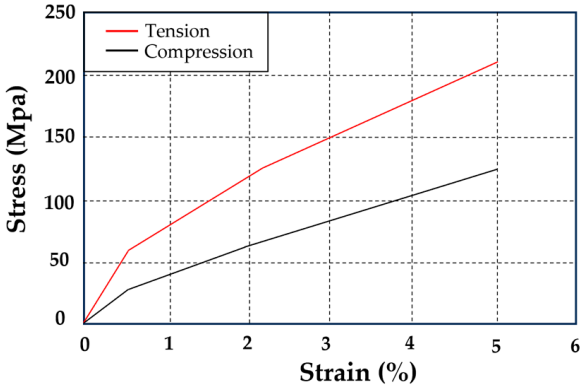

Figure 12. Calibrated trilinear asymmetric backbone curve with different responses of the tube in tension and compression as per the experimental test results by Hain [49,50].

6.1. Experimental Study Used for Validation of the Proposed Modeling Approaches

For the validation of the suggested modeling approach, an additional experiment was considered, the cyclic pushover test on the CFFT column with constant axial load by Shi [11].

Shi [11] conducted experiments involving constant axial load and cyclic lateral loads on a control RC column and five CFFTs with different fiber types, structures, and shear span-to-depth ratios. Among them, the Y specimen was a product of filament winding that utilized a commercially available GFRP tube with 75% glass content and was considered for model validation in this study. This GFRP tube consisted of winding of 17 layers of ±55° E-glass fibers and epoxy resin, with it having an inner diameter of 312 mm and a wall thickness of 5.5 mm. The column length of the Y specimen was 1295 mm as seen in Figure 13.

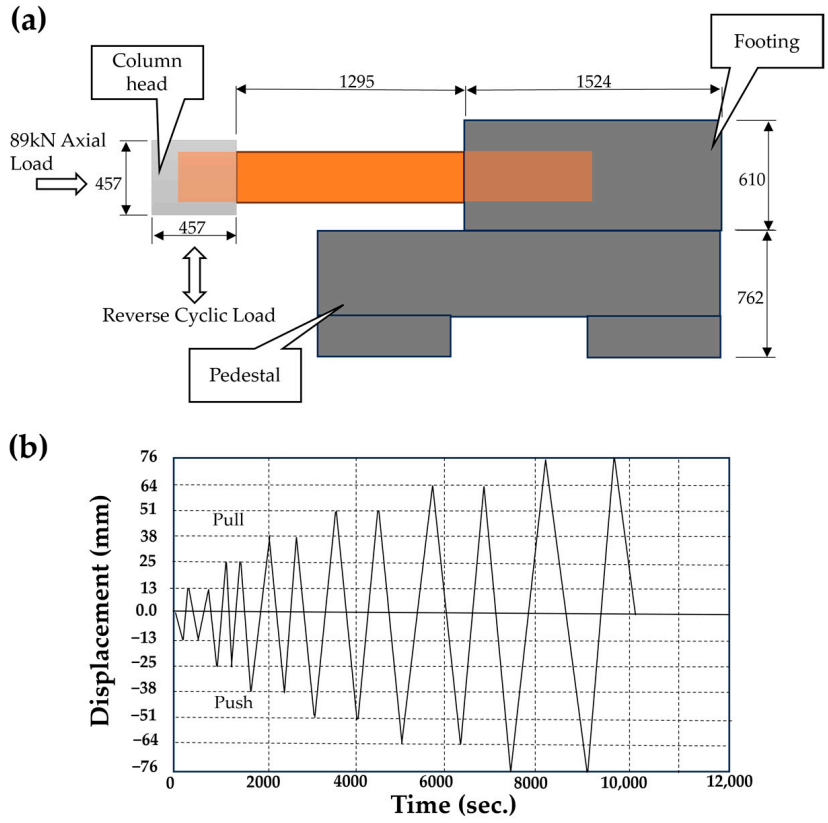

Figure 13. Experimental setup of the CFFT column by Shi [11]. (**a**) CFFT column with dimensions and applied loading conditions and (**b**) the reverse cyclic lateral loading protocol.

To replicate the effect of gravity loads on the columns, all specimens underwent external post-tensioning to 89 kN, equivalent to approximately $0.03 f'_c A_g$. The longitudinal mild steel reinforcement comprising sixteen 9.5 mm steel bars with a yield strength of 414 MPa was used. These bars extended the full length of the columns with 610 mm and 305 mm embedment into the footings and column heads, respectively. The longitudinal steel reinforcement ratio was 1.4% for specimen Y.

6.2. Results of Analytical Validation

The proposed two-pronged analytical modeling approach discussed earlier was implemented. Figure 14a demonstrates the effective alignment of the analytical hysteresis curve shape to the experimental result using Approach II with the Teng confinement model [20]. Meanwhile, Figure 14b accurately predicts the normalized peak moment value using Approach III with the Megalooikonomou confinement model [27] and the Paulay and Priestley [35] plastic hinge length model. Specifically, Approach III yields a prediction of 0.1, which closely matches the experimental value of 0.1004. Additionally, Approach III accurately represents the energy dissipation. The experimental normalized enclosed area is 30.1, while the predicted area is 30.8, resulting in a minor error of only 2.3%. Figure 14c represents the tri-linearization of the moment–curvature curve, obtained from the analysis performed in a fiber section, to be used in Approach III for representing the non-linear flexural behavior of the CFFT section.

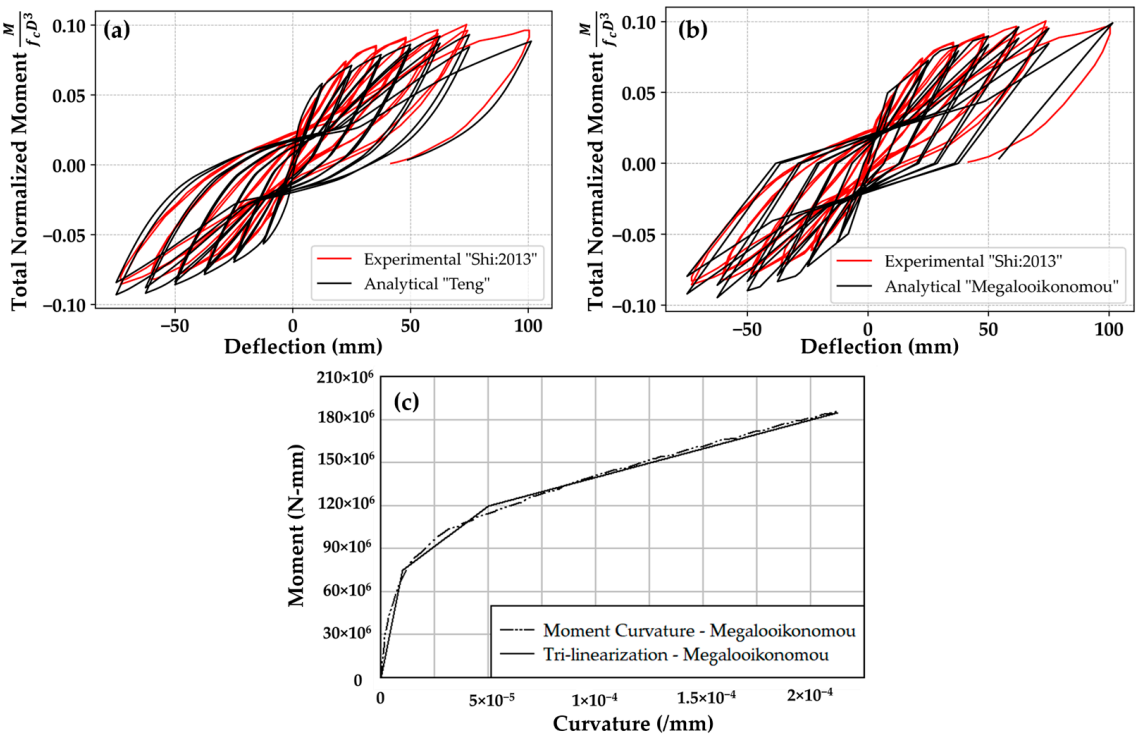

Figure 14. Validation of (**a**) Approach II with the Teng [20] confinement model, (**b**) Approach III with the Megalooikonomou [27] confinement model using the Paulay and Priestley [35] plastic hinge length model with respect to the experimental full cyclic hysteretic curve for the reverse cyclic transverse test on the CFFT beam-column by Shi [11], and (**c**) tri-linearization of the moment–curvature analysis performed in a fiber section.

7. Conclusions

This study applies and compares different analytical modeling approaches in OpenSeesPy3.5.1.12 and proposes their applicability in various scenarios to capture the cyclic behavior of concrete-filled ±55° GFRP tubes in lateral cyclic pushover loading and four-point bending with constant axial load. The key finding is that the distributed inelastic-

ity approach with a fiber element section to the plastic hinge zone when used in conjunction with the Teng confinement model [20] effectively predicts the shape of the hysteretic curve while maintaining computational efficiency. However, this analytical prediction remains in the slightly lower range than the experimental data due to the ignorance of confinement effects from the internal steel reinforcements. On the other hand, the lumped inelasticity modeling approach, based on the Paulay and Priestley plastic hinge length model [35], provides better estimates for the dissipated energy and peak load value of the full cyclic hysteretic curve. The Megalooikonomou [27] confinement model, which considers confinement effects from both the FRP tube and steel reinforcement, converges with the use of the lumped plasticity approach, accurately predicting the peak capacity and dissipated energy of the CFFT column. However, the shape of the hysteresis curve is multilinear, contradicting the experimental hysteretic curve shape.

These findings highlight the importance of considering confinement effects from both FRP tubes and internal steel reinforcements. Moving forward, the following areas for future research are recommended:

1. Enhanced FRP Confinement Model: Develop an improved FRP confinement model that accounts for contributions from both FRP and internal steel reinforcement. This model should address convergence issues while maintaining computational efficiency and capture the accurate shape of the hysteresis curve including precise predictions of both peak value and dissipated energy within finite element software OpenSeesPy3.5.1.12. This will enhance our understanding of the column's behavior under cyclic loading.
2. Experimental Validation: Conduct experimental tests to validate the proposed analytical models. Comparing the results with real-world behavior will enhance their reliability.
3. Application to Practical Design: Apply the developed models to practical design scenarios, considering different column geometries and loading conditions.
4. Material properties of FRP tubes: Conduct detailed investigations and experimental studies to understand the material properties of FRP tubes with varying fiber orientations in specific CFFT elements.

When designing CFFT columns with $\pm 55^{\circ}$ GFRP fiber orientation constructed with filament winding using the proposed modeling approaches, if the FRP material properties are unavailable, the longitudinal backbone curve for the FRP tube provided by Hain [49,50], the ultimate tensile stress of 71 MPa, and the longitudinal tensile elastic modulus of 12,548 MPa as adopted in the validation step of this study as provided by the manufacturer [51] can be considered.

Author Contributions: Conceptualization, S.S. and A.H.; methodology, S.S. and A.H.; software, S.S.; validation, S.S.; formal analysis, S.S. and A.H.; investigation, S.S. and A.H.; resources, A.H.; data curation, S.S.; writing—original draft preparation, S.S.; writing—review and editing, S.S. and A.H.; visualization, S.S. and A.H.; supervision, A.H.; project administration, A.H.; funding acquisition, A.H. All authors have read and agreed to the published version of the manuscript.

Funding: This research received no external funding; however, it utilized results from a project funded by the National Science Foundation Partnership for Innovation Award #1500293.

Data Availability Statement: The data that support the findings of this study are available from the corresponding author upon reasonable request.

Acknowledgments: We thank Konstantinos G. Megalooikonomou for fruitful technical discussions and support.

Conflicts of Interest: The authors declare no conflicts of interest.

References

1. Ortiz, J.D.; Khedmatgozar Dolati, S.S.; Malla, P.; Nanni, A.; Mehrabi, A. FRP-reinforced/strengthened concrete: State-of-the-art review on durability and mechanical effects. *Materials* **2023**, *16*, 1990. [CrossRef] [PubMed]
2. Zhu, Z.; Ahmad, I.; Mirmiran, A. Fiber element modeling for seismic performance of bridge columns made of concrete-filled FRP tubes. *Eng. Struct.* **2006**, *28*, 2023–2035. [CrossRef]
3. Zhu, Z.; Mirmiran, A.; Saiidi, M.S. Seismic performance of reinforced concrete bridge substructure encased in fiber composite tubes. *Transp. Res. Rec.* **2006**, *1976*, 197–206. [CrossRef]
4. Zaghi, A.E.; Saiidi, M.S.; Mirmiran, A. Shake table response and analysis of a concrete-filled FRP tube bridge column. *Comp. Struct.* **2012**, *94*, 1564–1574. [CrossRef]
5. Echevarria, A.E.; Zaghi, A.E.; Saiidi, M. Applicability of Concrete-Filled FRP Tube (CFFT) System for Multihazard Resilient Bridge Columns. *Struct. Cong* **2014**, *2014*, 441–452. [CrossRef]
6. Echevarria, A.; Zaghi, A.E.; Chiarito, V.; Christenson, R.; Woodson, S. Experimental comparison of the performance and residual capacity of CFFT and RC bridge columns subjected to blasts. *J. Bridge Eng.* **2016**, *21*, 04015026. [CrossRef]
7. Papavasileiou, G.S.; Megalooikonomou, K.G. Numerical simulation of FRP-confined circular bridge piers using OpenSees, Proc. In *OpenSees Days Italy (OSD), Second International Conference*; University of Salerno: Salerno, Italy, 2015.
8. Hain, A.; Zaghi, A.E.; Saiidi, M.S. Flexural behavior of hybrid concrete-filled fiber reinforced polymer tube columns. *Comp. Struct.* **2019**, *230*, 111540. [CrossRef]
9. Shao, Y.; Mirmiran, A. Experimental investigation of cyclic behavior of concrete-filled fiber reinforced polymer tubes. *J. Comp. Constr.* **2005**, *9*, 263–273. [CrossRef]
10. Zhu, Z.; Ahmad, I.; Mirmiran, A. Seismic performance of concrete-filled FRP tube columns for bridge substructure. *J. Bridge Eng.* **2006**, *11*, 359–370. [CrossRef]
11. Shi, Y.; Zohrevand, P.; Mirmiran, A. Assessment of Cyclic Behavior of Hybrid FRP Concrete Columns. *J. Bridge Eng.* **2013**, *18*, 553–563. [CrossRef]
12. Youm, K.; Cho, J.; Lee, Y.; Kim, J.J. Seismic performance of modular columns made of concrete filled FRP tubes. *Eng. Struct.* **2013**, *57*, 37–50. [CrossRef]
13. Ali, A.M.; Robillard, D.; Masmoudi, R.; Khan, I.M. Experimental investigation of bond and tube thickness effect on the flexural behavior of concrete-filled FPR tube under lateral cyclic loading. *J. King Saud Univ. Eng. Sci.* **2019**, *31*, 32–41. [CrossRef]
14. Lanning, A.; Hain, A.; Zaghi, A.E.; Saiidi, M.S. Experimental study on hybrid concrete-filled fiber reinforced polymer tube (HCFFTs) columns under simulated seismic loading. *Eng. Struct.* **2022**, *264*, 114478. [CrossRef]
15. Samaan, M.; Mirmiran, A.; Shahawy, M. Model of concrete confined by fiber composites. *J. Struct. Eng.* **1998**, *124*, 1025–1031. [CrossRef]
16. Saiid Saiidi, M.; Sureshkumar, K.; Pulido, C. Simple carbon-fiber-reinforced-plastic-confined concrete model for moment-curvature analysis. *J. Comp. Constr.* **2005**, *9*, 101–104. [CrossRef]
17. Youssef, M.N.; Feng, M.Q.; Mosallam, A.S. Stress–strain model for concrete confined by FRP composites. *Comp. Eng.* **2007**, *38*, 614–628. [CrossRef]
18. Lam, L.; Teng, J.G. Design-oriented stress–strain model for FRP-confined concrete. *Constr. Build. Mat.* **2003**, *17*, 471–489. [CrossRef]
19. Lam, L.; Teng, J.G. Stress–strain model for FRP-confined concrete under cyclic axial compression. *Eng. Struct.* **2009**, *31*, 308–321. [CrossRef]
20. Teng, J.G.; Jiang, T.; Lam, L.; Luo, Y.Z. Refinement of a design-oriented stress–strain model for FRP-confined concrete. *J. Comp. Constr.* **2009**, *13*, 269–278. [CrossRef]
21. Jiang, C.; Wu, Y.; Jiang, J. Effect of aggregate size on stress-strain behavior of concrete confined by fiber composites. *Compos. Struct.* **2017**, *168*, 851–862. [CrossRef]
22. Jiang, C. Strength enhancement due to FRP confinement for coarse aggregate-free concretes. *Eng. Struct.* **2023**, *277*, 115370. [CrossRef]
23. Ozbakkaloglu, T.; Lim, J.C.; Vincent, T. FRP-confined concrete in circular sections: Review and assessment of stress–strain models. *Eng. Struct.* **2013**, *49*, 1068–1088. [CrossRef]
24. Pessiki, S.; Harries, K.A.; Kestner, J.T.; Sause, R.; Ricles, J.M. Axial behavior of reinforced concrete columns confined with FRP jackets. *J. Comp. Constr.* **2001**, *5*, 237–245. [CrossRef]
25. Guo, H.; Yuan, H.; Zhang, J.; Ruan, D. Review of sandwich structures under impact loadings: Experimental, numerical, and theoretical analysis. *Thin-Walled Struct.* **2023**, *196*, 111541. [CrossRef]
26. Fahmy, M.F.; Ismail, A.M.; Wu, Z. Numerical study on the applicability of design-oriented models of FRP-confined concrete for predicting the cyclic response of circular FRP-jacketed RC columns. *J. Comp. Constr.* **2017**, *21*, 04017017. [CrossRef]
27. Megalooikonomou, K.G.; Monti, G.; Santini, S. Constitutive model for fiber-reinforced polymer-and tie-confined concrete. *ACI Struct. J.* **2012**, *109*, 569. [CrossRef]
28. Scott, M.H.; Fenves, G.L. Plastic hinge integration methods for force-based beam–column elements. *J. Struct. Eng.* **2006**, *132*, 244–252. [CrossRef]
29. Scott, M.H.; Ryan, K.L. Moment-rotation behavior of force-based plastic hinge elements. *Earth Spec.* **2013**, *29*, 597–607. [CrossRef]

30. Mackie, K.R.; Scott, M.H. Implementation of nonlinear elements for seismic response analysis of bridges. *Pract. Periodical Struct. Des. Constr.* **2019**, *24*, 04019011. [CrossRef]
31. Rahai, A.R.; Fallah Nafari, S. A comparison between lumped and distributed plasticity approaches in the pushover analysis results of a pc frame bridge. *Int. J. Civil. Eng.* **2013**, *11*, 217–225.
32. Pozo, J.D.; Hube, M.A.; Kurama, Y.C. Effective nonlinear simulations of RC columns with force-based elements. *J. Earthquake Eng.* **2023**, *27*, 340–361. [CrossRef]
33. Gu, D.; Wu, Y.; Wu, G.; Wu, Z. Plastic hinge analysis of FRP confined circular concrete columns. *Constr. Build. Mater.* **2012**, *27*, 223–233. [CrossRef]
34. Jiang, C.; Wu, Y.; Wu, G. Plastic hinge length of FRP-confined square RC columns. *J. Comp. Constr.* **2014**, *18*, 04014003. [CrossRef]
35. Paulay, T.; Priestley, M.N. *Seismic Design of Reinforced Concrete and Masonry Buildings*; John Wiley & Sons: New York, NY, USA, 1992; pp. 141–142.
36. Youssf, O.; ElGawady, M.A.; Mills, J.E. Displacement, and plastic hinge length of FRP-confined circular reinforced concrete columns. *Eng. Struct.* **2015**, *101*, 465–476. [CrossRef]
37. Yuan, F.; Wu, Y.; Li, C. Modelling plastic hinge of FRP-confined RC columns. *Eng. Struct.* **2017**, *131*, 651–668. [CrossRef]
38. Hisham, M.; Yassin, M. Nonlinear Analysis of Prestressed Concrete Structures under Monotonic and Cycling Loads. Ph.D. Dissertation, University of California, Berkeley, CA, USA, 1994.
39. Teng, J.G.; Lam, L.; Lin, G.; Lu, J.Y.; Xiao, Q.G. Numerical simulation of FRP-jacketed RC columns subjected to cyclic and seismic loading. *J. Comp. Constr.* **2016**, *20*, 04015021. [CrossRef]
40. Richard, R.M.; Abbott, B.J. Versatile elastic-plastic stress-strain formula. *J. Eng. Mech. Div.* **1975**, *101*, 511–515. [CrossRef]
41. Ahmad, S.H. Properties of Confined Concrete under Static and Dynamic Loads. Ph.D. Dissertation, University of Illinois at Chicago Circle, Chicago, IL, USA, 1981.
42. Ahmad, S.H.; Shah, S.P. Stress-strain curves of concrete confined by spiral reinforcement. *J. Proc.* **1982**, *79*, 484–490. [CrossRef]
43. Karsan, I.D.; Jirsa, J.O. Behavior of concrete under compressive loadings. *J. Struct. Div.* **1969**, *95*, 2543–2564. [CrossRef]
44. Triantafillou, T.; Matthys, S.; Audenaert, K.; Balázs, G.; Blaschko, M.; Blontrock, H.; Czaderski, C.; David, E.; Di Tomasso, A.; Duckett, W.; et al. *Externally Bonded FRP Reinforcement for RC Structures, Bulletin FIB 14*; International Federation for Structural Concrete (fib): Lausanne, Switzerland, 2001; pp. 1–130.
45. Braga, F.; Gigliotti, R.; Laterza, M. Analytical stress–strain relationship for concrete confined by steel stirrups and/or FRP jackets. *J. Struct. Eng.* **2006**, *132*, 1402–1416. [CrossRef]
46. Shao, Y. Seismic Performance of FRP-Concrete Beam-Column. Ph.D. Dissertation, North Carolina State University, Raleigh, NC, USA, 2003.
47. Mazzoni, S.; McKenna, F.; Scott, M.H.; Fenves, G.L. OpenSees command language manual. *Pac. Earthq. Eng. Res. (PEER) Cent.* **2006**, *264*, 137–158.
48. Megalooikonomou, K.G.; Monti, G. Numerical modeling of FRP-retrofitted circular RC columns including shear. In Proceedings of the 5th ECCOMAS Thematic Conference on Computational Methods in Structural Dynamics and Earthquake Engineering, Crete Island, Greece, 25 May 2015.
49. Hain, A.; Zaghi, A.E.; Lanning, A. Moment-Curvature Analysis of Hybrid Concrete-Filled Fiber Reinforced Polymer Tube Columns. *Struct. Cong* **2018**, *2018*, 338–348. [CrossRef]
50. Hain, A.; Motaref, S.; Zaghi, A.E. Influence of fiber orientation and shell thickness on the axial compressive behavior of concrete-filled fiber-reinforced polymer tubes. *Const. Build. Mat.* **2019**, *220*, 353–363. [CrossRef]
51. Fiber Glass Systems UL/ULC Listed Red Thread (R) IIA Piping Catalog. Available online: https://www.lbltrading.com/wp-content/uploads/2016/12/Red-Thread-IIA-piping-catalog-Fibercast.pdf (accessed on 1 October 2007).